Searching for a continuum limit in causal dynamical triangulation quantum gravity

J. Ambjørn,[1,2,*] D. N. Coumbe,[1,3,†] J. Gizbert-Studnicki,[3,‡] and J. Jurkiewicz[3,§]

[1]*The Niels Bohr Institute, Copenhagen University, Blegdamsvej 17, DK-2100 Copenhagen Ø, Denmark*
[2]*IMAPP, Radboud University, Heyendaalseweg 135, 6525 AJ Nijmegen, The Netherlands*
[3]*Institute of Physics, Jagiellonian University, ulica professor Stanislawa Lojasiewicza 11,
PL 30-348 Krakow, Poland*

We search for a continuum limit in the causal dynamical triangulation approach to quantum gravity by determining the change in lattice spacing using two independent methods. The two methods yield similar results that may indicate how to tune the relevant couplings in the theory in order to take a continuum limit.

I. INTRODUCTION

Causal dynamical triangulations (CDT) define a nonperturbative approach to quantum gravity in which spacetime is divided into a lattice of four-dimensional Lorentzian triangles. At first sight this seems to suggest that CDT defines a discrete spacetime; however, the hope is that one can study spacetime on lattices of ever decreasing edge length, with the eventual aim of investigating the properties of spacetime in the continuum limit. It is therefore important to be able to reliably determine the lattice spacing in CDT, as well as how it changes within the parameter space. In this work we calculate the lattice spacing using two independent methods at a number of different points in the parameter space with the aim of gaining an insight into how one might take a continuum limit in CDT.

As is well known, gravity as a perturbative quantum field theory is not renormalizable by power counting [1]. However, as suggested in Weinberg's seminal work [2] the definition of renormalizability might be generalized to the nonperturbative regime as detailed by the asymptotic safety scenario [3]. The asymptotic safety scenario would be realized if a finite number of couplings terminated at an ultraviolet fixed point (UVFP) so that the theory remains finite and predictive even in the infinite energy limit; there is now a growing body of evidence supporting the existence of such an UVFP [4–8]. In this way a lattice theory of gravity, such as CDT, might also be used to provide evidence for asymptotic safety by searching for a second-order critical point in its parameter space which would correspond to an UVFP. The divergent correlation length characteristic of a second-order critical point would allow for the possibility of taking the lattice spacing to zero while

simultaneously keeping observable quantities fixed in physical units.

A defining feature of CDT is the existence of a causality condition that allows one to distinguish between spacelike and timelike links on the lattice. The existence of a causality condition allows the foliation of the lattice into spacelike hypersurfaces of fixed topology. There exist two types of four-dimensional triangulations in CDT, the (4,1)-simplex and the (3,2)-simplex, where the notation (i, j) refers to the number of vertices i on hypersurface t, and the number of vertices j on hypersurface $t \pm 1$. In CDT the lattice spacing of timelike links a_t and that of spacelike links a_s are not necessarily equal but are related via a α parameter

$$a_t^2 = -\alpha a_s^2. \tag{1}$$

For $\alpha = -1$ we have $a_t = a_s$. By taking $\alpha \neq -1$ and following Regge's method for describing piecewise linear geometries [9], we obtain a simple expression for the Einstein-Hilbert action of CDT [10],

$$S_E = -(\kappa_0 + 6\Delta)N_0 + \kappa_4(N_{(4,1)} + N_{(3,2)}) + \Delta N_{(4,1)}, \tag{2}$$

where κ_0 is proportional to a_s^2/G and G is the bare Newton constant. The parameter Δ is related to the ratio of spacelike and timelike links on the lattice, and κ_4 is related to the cosmological constant, which is fixed so one can extrapolate to the infinite volume limit. We can then independently vary κ_0 and Δ in order to explore the parameter space of CDT.

The key features of the CDT parameter space have by now been largely mapped out. It has been demonstrated that phase C has semiclassical features that closely resemble four-dimensional de Sitter space [11,12]. The solid red line in Fig. 1, originally thought to separate phase B from phase C, appears to be a second-order transition [13], allowing for the possibility of taking a continuum limit. However, the location of the newly discovered bifurcation phase [14] separating phase C from phase B may prevent the

*[*]ambjorn@nbi.dk
[†]daniel.coumbe@nbi.ku.dk
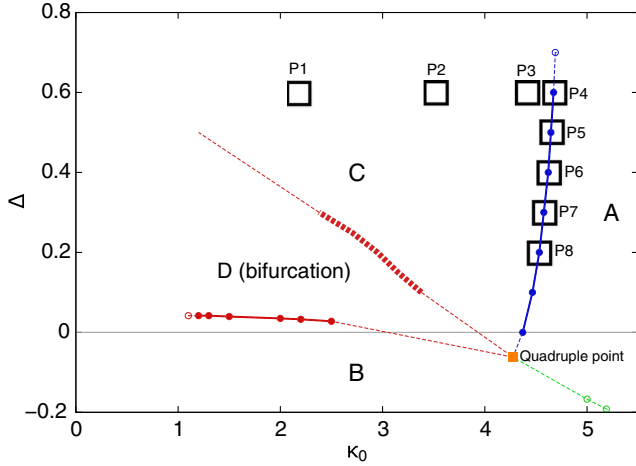[‡]jakub.gizbert-studnicki@uj.edu.pl
[§]jerzy.jurkiewicz@uj.edu.pl

FIG. 1.   A schematic representation of the parameter space of CDT. The colored circles represent measured phase transition points and the colored lines their interpolation. The open black squares denote the eight points in the parameter space which we study in this work.

possibility of approaching the second-order transition line from within the physically interesting phase C (see Fig. 1). Furthermore, recent studies suggest the continuum limit may exist for sufficiently large κ_0 and Δ, rather than near the B-C transition as previously thought [15]. The aim of this work is to independently check the findings of Ref. [15] by determining how the lattice spacing changes as a function of the bare parameters κ_0 and Δ using two independent methods.

II. SIMULATION DETAILS

The first of the two methods we use to determine the effective lattice spacing in this work is based on analyzing fluctuations of three-volume, as first introduced in Refs. [12] and [11]. This method relies on the observation that within phase C of the CDT parameter space, the distribution of three-volume as a function of time has an expectation value that closely matches de Sitter space. Since the classical solution for de Sitter space does not contain Newton's constant but the semiclassical fluctuations about de Sitter space do, one can exploit this fact to estimate the lattice spacing in Planck units for each point in phase C of the parameter space. We defer a detailed discussion of this method to Sec. III. The second of our two methods involves measurements of the so-called spectral dimension, a measure of the effective fractal dimension of a geometry. In CDT, the spectral dimension $D_S(\sigma)$ is defined via a discrete diffusion process and is related to the probability $P_r(\sigma)$ that a random walk on the geometry returns to its origin after σ diffusion steps. In this work we calculate the spectral dimension $D_S(\sigma)$ as a function of σ for a number of different points in phase C of the CDT parameter space. As detailed in Sec. IV, a

comparison of $D_S(\sigma)$ at different points in the parameter space can then be used to determine the effective change in lattice spacing.

We aim to reduce systematic errors associated with our measurements in two ways. First, we aim to reduce finite size effects. In Ref. [16], finite size effects were shown to be negligible for lattice volumes of $N_{4,1} = 160$ k for the bare parameters $(\kappa_0 = 2.2, \Delta = 0.6)$, $(\kappa_0 = 3.6, \Delta = 0.6)$, and $(\kappa_0 = 4.4, \Delta = 0.6)$. However, for bare parameters corresponding to finer lattice spacings finite-size effects appeared to increase. For this reason we simulate with a larger lattice volume $N_{(4,1)} = 300$ k close to the C-A transition line in order to reduce finite size effects. Second, the discretization effects of odd-even oscillations in the short-distance spectral dimension have been removed by omitting values of $D_S(\sigma)$ from the fit functions wherever they become significant, as indicated in Fig. 3; typically this occurs around $\sigma \approx 80$.

We reduce statistical errors by ensuring that our configurations are thermalized. This check is made by analyzing $D_S(\infty)$ as a function of Monte Carlo time and showing that there is no statistical difference between the first and second halves of the measured data set, as detailed in Ref. [16].

The spectral dimension in this work is determined by taking the starting point of diffusion processes to be in the time slice containing the maximal number of (4,1)-simplices, so as to ensure that we are probing the bulk geometry with each diffusion. The maximal number of time steps σ in our calculations is set to 500, and the time extension of our ensembles is $t = 80$. We use a linear volume fixing constraint $\delta S = \epsilon |N_{(4,1)} - N_{(4,1)}^{\text{target}}|$, with $\epsilon = 0.02$ after thermalization when determining the change in lattice spacing described in Sec. IV. For technical convenience we use a quadratic volume fixing constraint $\delta S = \epsilon (N_{(4,1)} - N_{(4,1)}^{\text{target}})^2$, with $\epsilon = 0.00001$ when determining the lattice spacing described in Sec. III.[1]

The (κ_0, Δ) coordinates of the points at which we simulate in this work are schematically depicted in Fig. 1.

III. METHOD 1: FLUCTUATIONS AROUND DE SITTER SPACE

In order to perform numerical simulations one typically has to work with dimensionless quantities by expressing all parameters in terms of the (absolute) lattice spacing a_{abs}

---

[1]In order to determine the absolute lattice spacing, we fit the parameters of the effective action as described in Sec. III. This is done by analyzing the inverse of the covariance matrix of spatial volume fluctuations. To get rid of the zero mode and make the matrix invertible, we allow for total volume fluctuations around $N_{(4,1)}^{\text{target}}$ and subtract the effect of volume fixing from the effective action. For the quadratic volume fixing the effect is a simple shift of the inverse matrix elements by a constant 2ϵ.

and then assuming $a_{abs} = 1$. As a result, in order to translate (dimensionless) numerical results into (dimensionful) physical units, one should find a way to measure the absolute lattice spacing. This can be achieved by looking at effective observables and comparing them to corresponding physical constants, which reintroduces a scale into the numerical system.

The method for determining the absolute lattice spacing that we study in this section was first proposed in Refs. [11,12]. It is based on the observation that inside phase C of the CDT parameter space, the distribution of volume as a function of time has an expectation value that closely matches de Sitter space and hence closely resembles a maximally symmetric spacetime with a positive cosmological constant with 3-volume distributed according to the universal curve [12]

$$\langle N_3(t) \rangle = \frac{3}{4} \frac{N_{(4,1)}}{s_0 N_{(4,1)}^{1/4}} \cos^3\left(\frac{t}{s_0 N_{(4,1)}^{1/4}}\right). \qquad (3)$$

$N_3(t)$ is (twice) the number of tetrahedra[2] comprising each spatial slice at a (discrete) time t, where the result is independent of the total lattice volume. The constant s_0 depends on the radius of the extended part of the universe (the so-called *blob*). At the same time quantum fluctuations $\delta N_3(t) = N_3(t) - \langle N_3(t) \rangle$ are consistent with the effective action [12]

$$S_{\text{eff}} = \frac{1}{\Gamma} \sum_t \left(\frac{(N_3(t+1) - N_3(t))^2}{N_3(t+1) + N_3(t)} + \mu N_3(t)^{1/3} - \lambda N_3(t) \right), \qquad (4)$$

where Γ is a dimensionless constant depending on the amplitude of quantum fluctuations.

In this section we assume the CDT universe measured inside phase C is that of Euclidean de Sitter space (four-sphere) with superimposed quantum fluctuations of the spatial volume obtained for a spatially isotropic and homogeneous metric, having a line element

$$ds^2 = g_{\tau\tau}d\tau^2 + a^2(\tau)d\Omega^3. \qquad (5)$$

The Einstein-Hilbert action calculated for the metric (5) becomes a minisuperspace (MS) action which can be parametrized by a spatial volume observable $V_3(\tau) = \int d\Omega_3 \sqrt{g}|_{S^3} = 2\pi^2 a^3(\tau)$ in the following form:

$$S_{\text{MS}} = \frac{1}{24\pi G} \int d\tau \sqrt{g_{\tau\tau}} \left(\frac{g^{\tau\tau}(\partial_\tau V_3(\tau))^2}{V_3(\tau)} \right.$$
$$\left. + \tilde{\mu} V_3(\tau)^{1/3} - \tilde{\lambda} V_3(\tau) \right), \qquad (6)$$

where G is the dimensionful ($[G] = L^2$) Newton constant. For the MS action (6) the semiclassical spatial volume profile is given by

$$\langle V_3(\tau) \rangle = 2\pi^2 \mathcal{R}^3 \cos^3\left(\frac{\sqrt{g_{\tau\tau}}\tau}{\mathcal{R}}\right) = \frac{3}{4} \frac{V_4}{\tilde{s}_0 V_4^{1/4}} \cos^3\left(\frac{\sqrt{g_{\tau\tau}}\tau}{\tilde{s}_0 V_4^{1/4}}\right), \qquad (7)$$

where $\mathcal{R}$ is the radius and $V_4 = \frac{8\pi^2}{3}\mathcal{R}^4$ is the total 4-volume of the four-sphere [and $\tilde{s}_0 = (\frac{3}{8\pi^2})^{1/4}$].

A natural identification of discrete expressions (3) and (4) with their continuous counterparts (7) and (6), respectively, via simple dimensional analysis leads to the conclusion that

$$l_{pl}^2 \equiv G \propto \Gamma \cdot a_{abs}^2, \qquad (8)$$

where $l_{pl} = \sqrt{G}$ is the Planck length (in units $\hbar = c = 1$) and a_{abs} is the physical lattice spacing. The dimensionless proportionality factor in (8) is derived in Appendix A, giving the formula for absolute lattice spacing that we will use in this section, namely,

$$a_{abs} = \sqrt{\frac{3\sqrt{6}}{\sqrt{C_4} s_0^2 \Gamma}} l_{pl}, \qquad (9)$$

where C_4 is the dimensionless *effective* volume of a unit 4-simplex, while s_0 is the extension of the universe defined by Eq. (3) and Γ is the amplitude of quantum fluctuations defined by Eq. (4). In order to estimate s_0 we make a fit of Eq. (3) to the average volume profile $\langle N_3(t) \rangle$ measured in numerical simulations. The procedure of estimating Γ is based on the analysis of the covariance matrix $C_{tt'} \equiv \langle \delta N_3(t) \delta N_3(t') \rangle$, where $\delta N_3(t) \equiv N_3(t) - \langle N_3(t) \rangle$, and it follows the procedure described in detail in Ref. [17]. We use the inverse of the empirical covariance matrix $C_{tt'}^{-1}$, whose elements are (in a semiclassical approximation) given by second-order derivatives of the effective action (4), to fit the action parameters to numerical data.

We use three methods for determining a_{abs}. Each method uses formula (9) but differs in the way C_4 is determined (the measurement of s_0 and Γ is universal). The three methods are as follows (see Appendix A for more details):

(i) In method (a) we set $C_4 = \text{const.}$ (independent of the position in CDT parameter space). This is consistent with the assumption that spatial layers of equal (integer) t, which are built of equilateral tetrahedra, are separated by a universal time distance of constant lattice length. As such, tetrahedra are constituents (faces) of (4,1)-simplices; in this approach one takes into account only simplices of this type, disregarding all (3,2)-simplices.

(ii) In method (b) we assume $C_4 = C_4(\xi)$, where $\xi = N^{(3,2)}/N^{(4,1)}$. In Ref. [17] it was shown that

---

[2]Note that in order to have $\sum_t N_3(t) = N_{(4,1)}$ we set $N_3(t) \equiv N_{(4,1)}(t) = 2N_{\text{tetrahedra}}(t)$.

(3,2)-simplices form closed layers which can be attributed to a half-integer t variable. The number of (3,2)-simplices in each layer is consistent with the volume profile of (4,1)-simplices (tetrahedra) in integer t by a simple rescaling of ξ. This method is more general than (a), as it takes into account both (4,1)- and (3,2)-simplicial layers. A simplification and approximation comes from the fact that one assumes that all 4-simplices are symmetric and thus the volume of each 4-simplex is constant and universal, independent of the position in the parameter space ($C_{41} = C_{32} = \mathrm{const.}$).

(iii) In method (c) we assume $C_4 = C_4(\xi, C_{41}, C_{32})$, where $\xi = N^{(3,2)}/N^{(4,1)}$. This is the most general assumption as it accounts for the fact that the volume of a unit 4-simplex depends on the position in the bare parameter space of CDT and, in principle, $C_{41}(\alpha) \neq C_{32}(\alpha)$. This method requires determining the value of the parameter $\alpha = \alpha(\kappa_0, \Delta, \kappa_4)$ which defines the asymmetry between the length of timelike and spacelike links on the lattice.

The reason for using various methods is due to the fact that we want to compare the results of the absolute lattice spacing derived in this section with the relative lattice spacing defined by the rescaling of the spectral dimension (see Sec. IV), and check which method gives the closest agreement. Additionally, method (c), which naively seems to be the most accurate, breaks down close to the C-A phase transition (where double-valued or complex α solutions are possible).

In principle, all three parameters in formula (9), s_0, Γ and C_4 [in methods (b) and (c)] depend on the actual position in the CDT bare parameter space. As a result $a_{abs} = a_{abs}(\kappa_0, \Delta, \kappa_4)$. One can check how a_{abs} changes by
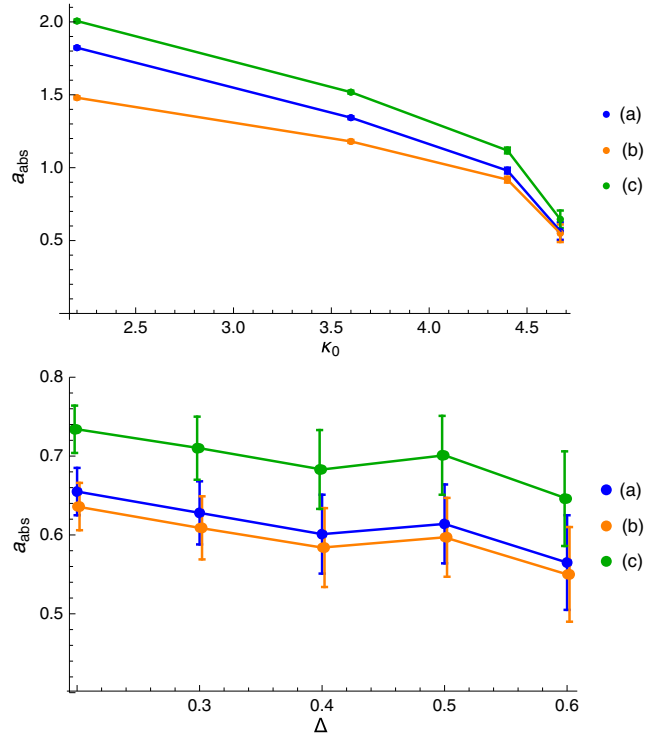

FIG. 2. Visualization of the data in Table I. The top chart shows the dependence of a_{abs} on κ_0 for fixed $\Delta = 0.6$, and the bottom chart shows the dependence of a_{abs} on Δ along the C-A phase transition line. Note that the scale is different in each chart.

following various trajectories in the parameter space and determining those for which $a_{abs} \to 0$ monotonically. The values of a_{abs} at each sampled point of the bare parameter space in phase C are presented in Table I and Fig. 2, where we compare the absolute lattice spacing calculated using the three different methods described. The error bars shown in Table I and Fig. 2 are related to fitting errors of parameters Γ, s_0 and ξ used to calculate a_{abs} by formula (9) and do not take into account statistical errors. The error bars clearly increase close to the C-A phase transition, which is mainly due to the increased error associated with Γ. $\Gamma \to \infty$ as one approaches the phase transition, resulting in a high signal-to-noise ratio in the measured inverse covariance matrix, which produces the increased error estimate.

IV. METHOD 2: RESCALING OF THE SPECTRAL DIMENSION

The spectral dimension is related to the probability $P_r(\tilde{\sigma})$ that a random walk returns to the origin after a fictitious diffusion time $\tilde{\sigma}$. The spectral dimension can be derived from the d-dimensional diffusion equation

$$\frac{\partial}{\partial \tilde{\sigma}} K_g(\zeta_0, \zeta, \tilde{\sigma}) - g^{\mu\nu}\nabla_\mu \nabla_\nu K_g(\zeta_0, \zeta, \tilde{\sigma}) = 0, \quad (10)$$

where K_g is the heat kernel defining the probability density of diffusing between ζ_0 and ζ. Here ∇ is the covariant

TABLE I. The table shows a_{abs} for eight points (κ_0, Δ) in phase C of the CDT parameter space. The absolute lattice spacing a_{abs} was determined by analyzing fluctuations about de Sitter space using three different methods, (a), (b) and (c), described in the text. The lattice spacing is in units of the Planck length l_{pl}.

Label in Fig. 1	(κ_0, Δ)	a_{abs} (a)	a_{abs} (b)	a_{abs} (c)
P1	(2.20,0.6)	1.82 ± 0.01	1.48 ± 0.01	2.01 ± 0.01
P2	(3.60,0.6)	1.34 ± 0.01	1.18 ± 0.01	1.52 ± 0.01
P3	(4.40,0.6)	0.98 ± 0.02	0.92 ± 0.02	1.12 ± 0.02
P4	(4.67,0.6)	0.56 ± 0.06	0.55 ± 0.06	0.65 ± 0.06
P5	(4.64,0.5)	0.61 ± 0.05	0.60 ± 0.05	0.70 ± 0.05
P6	(4.62,0.4)	0.60 ± 0.04	0.58 ± 0.04	$0.68 \pm 0.04^*$
P7	(4.57,0.3)	0.63 ± 0.04	0.61 ± 0.04	$0.71 \pm 0.04^*$
P8	(4.53,0.2)	0.65 ± 0.03	0.64 ± 0.03	$0.73 \pm 0.03^*$

For the last three points method (c) breaks down, as there exist two real solutions for α (with $\alpha < 1$ and $\alpha \gg 1$) and thus two solutions for a_{abs} (among the two, we have chosen the one with $\alpha < 1$, which is also the case for the points where only one solution is possible—this fact is denoted by "").

derivative of the metric $g_{\mu\nu}$. For infinitely flat Euclidean space, Eq. (10) has the solution

$$K_g(\zeta_0, \zeta, \tilde{\sigma}) = \frac{\exp\left(-d_g^2(\zeta, \zeta_0)/4\tilde{\sigma}\right)}{(4\pi\tilde{\sigma})^{d/2}}, \qquad (11)$$

where $d_g^2(\zeta, \zeta_0)$ defines the geodesic distance between ζ and ζ_0.

The quantity that is measured in the numerical simulations is the probability of return $P_r(\tilde{\sigma})$, which in asymptotically flat space is given by

$$P_r(\tilde{\sigma}) = \frac{1}{\tilde{\sigma}^{d/2}}. \qquad (12)$$

The scale-dependent spectral dimension $D_S(\tilde{\sigma})$ is then computed by taking the logarithmic derivative with respect to $\tilde{\sigma}$,

$$D_S(\tilde{\sigma}) = -2\frac{d\log\langle P_r(\tilde{\sigma})\rangle}{d\log\tilde{\sigma}}. \qquad (13)$$

In CDT, Euclidean space is discretized by a simplicial manifold, and the diffusion time $\tilde{\sigma}$ is counted by the number of discrete diffusion steps σ on the dual lattice; i.e., each diffusion step consists of moving from the center of one 4-simplex to the center of a neighboring 4-simplex. One starts the diffusion process from a randomly chosen simplex and numerically calculates the probability of return to the origin $P_r(\sigma)$ after σ diffusion steps. Measured values of $P_r(\sigma)$ are averaged over different starting points and different triangulations, and then one uses a discrete version of Eq. (13) to calculate $D_S(\sigma)$.

In a lattice formulation of an asymptotically safe field theory, an ultraviolet fixed point is expected to manifest as a second-order critical point. At a second-order critical point macroscopic observables become independent of the microscopic regularization and should therefore become scale invariant. A scale-invariant spectral dimension would appear as a perfectly flat $D_S(\sigma)$ curve over all distance scales σ. Therefore, we should expect to see progressively flatter spectral dimension curves as we approach such a fixed point. The amount by which we must rescale $D_S(\sigma)$ at a particular point in the parameter space such that it agrees with $D_S(\sigma)$ at another point in the parameter space will then be related to the change in relative lattice spacing when transforming between the two points, a method first proposed in Ref. [16].

To test the validity of this method we calculate the spectral dimension for eight different points in the parameter space (see Fig. 1) and compare the results with those obtained using the independent method of calculating the absolute lattice spacing via fluctuations about de Sitter space as described in Sec. III. Our results for the spectral dimension as a function of diffusion time for the eight points sampled in the parameter space are presented in Fig. 3. Typically, we find a small scale spectral dimension
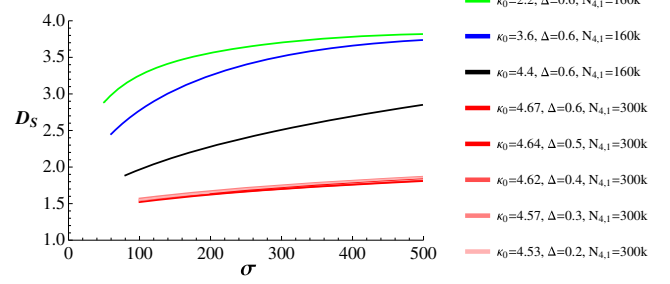

FIG. 3. The spectral dimension $D_S(\sigma)$ as a function of diffusion time σ for eight different points in phase C of the CDT parameter space.
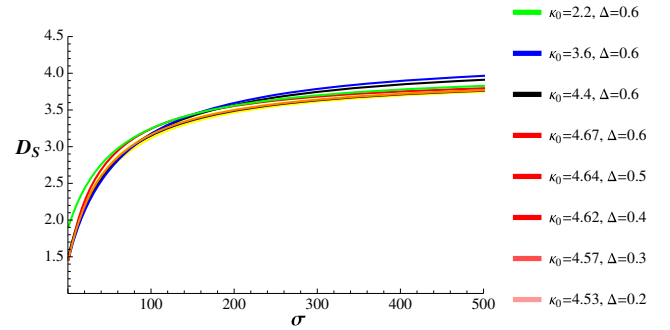

FIG. 4. The spectral dimension fits rescaled according to $D_S(\sigma) = a - \frac{b}{c+\sigma/a_{\text{rel}}^2}$, where a_{rel} is chosen such that the curves give the best overlap.

that is more consistent with the lower bound $D_S(\sigma \to 0) \sim 3/2$ (see Ref. [16] for typical error estimates) than with $D_S(\sigma \to 0) \simeq 2$, thereby supporting the findings of Ref. [16]. Furthermore, except for the points close to the C-A transition, we find a large scale spectral dimension that is consistent with $D_S(\sigma \to \infty) \sim 4$.

Within phase C of CDT, the fit function

$$D_S(\sigma) = a - \frac{b}{c + \sigma} \qquad (14)$$

has been shown to accurately fit the spectral dimension data [16,18], a result that is also supported by purely analytic models [19]. In Fig. 4 we rescale the fit function according to[3]

$$D_S(\sigma) = a - \frac{b}{c + \sigma/a_{\text{rel}}^2}, \qquad (15)$$

where a_{rel} is chosen such that the curves give the best overlap. The curves are normalized such that the scale factor a_{rel} is set to unity for the point $(\kappa_0 = 2.2, \Delta = 0.6)$

---

[3]In order to compare the results of a_{rel} with the absolute lattice spacing a_{abs}, one should rescale σ by a_{rel}^2 due to the squared covariant derivative of the metric in Eq. (10).

TABLE II. The table shows a_{rel} for eight points in phase C of the CDT parameter space. The values of a_{rel} are normalized such that $a_{\text{rel}} = 1$ for the point $(\kappa_0 = 2.2, \Delta = 0.6)$, a choice which is of course arbitrary. For comparison we also show the lattice spacing a_{abs} rescaled [independently for each of the methods (a), (b) and (c)] such that $a_{abs} = 1$ for the point $(\kappa_0 = 2.2, \Delta = 0.6)$.

Label in Fig. 1	(κ_0, Δ)	a_{rel}	a_{abs} (a)	a_{abs} (b)	a_{abs} (c)
P1	(2.20,0.6)	1	1	1	1
P2	(3.60,0.6)	0.791 ± 0.008	0.74 ± 0.01	0.80 ± 0.01	0.76 ± 0.01
P3	(4.40,0.6)	0.336 ± 0.006	0.54 ± 0.01	0.62 ± 0.02	0.56 ± 0.01
P4	(4.67,0.6)	0.116 ± 0.001	0.31 ± 0.03	0.37 ± 0.04	0.32 ± 0.03
P5	(4.64,0.5)	0.134 ± 0.001	0.34 ± 0.03	0.40 ± 0.04	0.35 ± 0.03
P6	(4.62,0.4)	0.118 ± 0.003	0.33 ± 0.02	0.40 ± 0.03	0.34 ± 0.02
P7	(4.57,0.3)	0.122 ± 0.001	0.34 ± 0.02	0.41 ± 0.03	0.35 ± 0.02
P8	(4.53,0.2)	0.122 ± 0.001	0.36 ± 0.02	0.43 ± 0.02	0.37 ± 0.02

[this choice is arbitrary since any pair of (κ_0, Δ) values could be defined as the point relative to which all other points are compared]. The resulting values of a_{rel} and their associated error estimates at each sampled point in the parameter space are shown in Table II.

Since we wish to minimize systematic errors associated with determining a_{rel}, we make a statistical comparison between the spectral dimension curves we wish to compare. We calculate the standard deviation by comparing central data points for $D_S(\sigma)$ at 10 different σ values for our canonical point $(\kappa_0 = 2.2, \Delta = 0.6)$ with the rescaled $D_S(\sigma)$ at our comparison point. To reduce discretization effects we only compare values for which $\sigma \geq 100$. We compare 10 evenly spaced $D_S(\sigma)$ values between $\sigma = 100$ and $\sigma = 460$. We determine the corrected sample standard deviation S via

$$S = \sqrt{\frac{\sum_{j=0}^{j=9} (D_S(\sigma = 100 + 40j) - D_S^C(\sigma = 100 + 40j))^2}{n-1}},$$

(16)

where $D_S^C(\sigma)$ is the spectral dimension at the canonical point $(\kappa_0 = 2.2, \Delta = 0.6)$ and $D_S(\sigma)$ is the rescaled spectral dimension curve with which we make the comparison, e.g., $(\kappa_0 = 3.6, \Delta = 0.6)$, and n is the number of compared points. Using this method we can determine how the standard deviation S varies as a function of a_{rel}, as shown by the black curve in Fig. 5. The value of a_{rel} for which S is minimized, as indicated by the black dashed vertical line in Fig. 5, then corresponds to the value of a_{rel} for which the curves give the best overlap.

It is important to estimate the errors associated with determining the relative lattice spacing. To estimate this error we calculate S as a function of a_{rel} by comparing the minimum possible values of $D_S(\sigma)$ allowed by the error bars with the maximum possible values of $D_S^C(\sigma)$ allowed by the error bars, as shown by the red curve in Fig. 5, which is calculated by comparing $D_S(\sigma)$ values at the points $(\kappa_0 = 3.6, \Delta = 0.6)$ and $(\kappa_0 = 2.2, \Delta = 0.6)$.

The difference in the values of a_{rel} for which the red and black curves are minimized then gives an estimate of the error associated with a_{rel}. For the points close to the C-A transition we typically find $D_S(\sigma \to \infty) < 4$, and so to aid a better comparison with $D_S^C(\sigma)$ we constrain $a \approx 4$ in the fit function while still ensuring a good fit to the data. Furthermore, for the points close to the C-A transition we compare only the central values of $D_S(\sigma)$ with the central and maximal values of $D_S^C(\sigma)$; consequently, the error estimate associated with a_{rel} for the points close to the C-A transition is likely to be significantly underestimated.
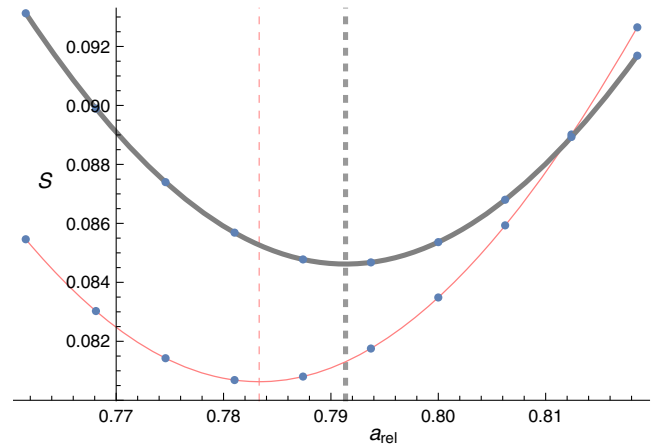

FIG. 5. The standard deviation S (filled dots) calculated by comparing $D_S(\sigma)$ at $(\kappa_0 = 2.2, \Delta = 0.6)$ with the rescaled curve at $(\kappa_0 = 3.6, \Delta = 0.6)$ as a function of a_{rel}. An interpolating function has been used to smoothly interpolate between data points. The value of a_{rel} for which the solid black curve is minimized yields the best overlap between the two $D_S(\sigma)$ curves. The solid red curve is determined by comparing the minimum values of $D_S(\sigma)$ allowed by the error bars at the point $(\kappa_0 = 3.6, \Delta = 0.6)$ with the maximal values of $D_S(\sigma)$ allowed within error bars at the point $(\kappa_0 = 2.2, \Delta = 0.6)$. The difference in the minimum of these two curves gives an estimate of the error associated with a_{rel}.
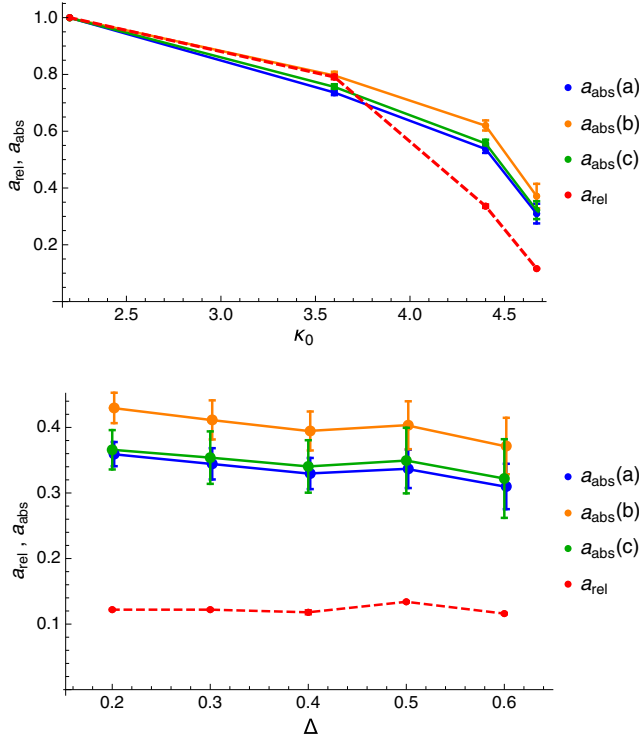
FIG. 6. Visualization of data from Table II. The lattice spacing data are normalized such that $a = 1$ for the point ($\kappa_0 = 2.2$, $\Delta = 0.6$). The top chart shows the dependence of a_{abs} and a_{rel} on κ_0 for fixed $\Delta = 0.6$. The bottom chart shows the dependence of a_{abs} and a_{rel} on Δ close to the C-A phase transition line.

V. INDICATIONS OF A CONTINUUM LIMIT

The changes in lattice spacing determined by analyzing fluctuations about de Sitter space and by rescaling the spectral dimension both indicate the lattice spacing is strongly dependent on κ_0, but that it is either independent or only very weakly dependent on Δ. The results summarized in Table II and Fig. 6 suggest that maximizing κ_0 within phase C is predominately responsible for minimizing the lattice spacing. Since the C-A transition defines the line of maximal κ_0 values in phase C, it should also then define the set of points for which the lattice spacing is minimized for any given Δ value. Extrapolating the measured transition points along the C-A line over the entire Δ range suggests that κ_0 is maximized within phase C for very large, possibly infinite Δ. If this scenario is correct it suggests one should tune the bare parameters to the C-A transition and move in the direction of increasing Δ in order to approach the continuum limit.[4]

The data presented in this work suggest the lattice spacing in phase C is minimized when κ_0 is maximized

---

[4]It is unlikely that one can take a continuum limit anywhere on the C-A transition itself since it is almost certainly first order [20]; however, it may be that the C-A transition terminates at a second-order critical point for some Δ value, just as it appears to do at the quadrupole point (see Fig. 1).
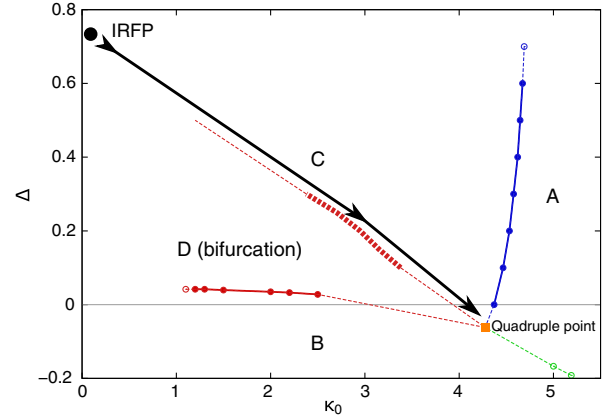

FIG. 7. A possible renormalization group trajectory in phase C of CDT. The trajectory flows from an IRFP in the direction of decreasing lattice spacing (as indicated by the arrows), as inferred from calculations of a_{abs} and a_{rel} at eight different points in the parameter space (as shown in Fig. 1).

within phase C, which implies one must tune to the C-A transition line to take a continuum limit. Conversely, the point at which κ_0 is minimized within phase C may then be a candidate for an infrared fixed point (IRFP). Based on our current picture of the CDT parameter space (Fig. 1) such an IRFP would exist on the transition line dividing phase C and the bifurcation phase for the minimal allowed value of κ_0. Our measurements may then be interpreted as suggesting a renormalization group trajectory within the parameter space shown schematically in Fig. 7.

VI. DISCUSSION AND CONCLUSIONS

If causal dynamical triangulation is to be a viable candidate for a nonperturbative theory of quantum gravity, then the expectation is that it should realize the asymptotic safety scenario for gravity. If CDT is to realize the asymptotic safety scenario, then it should contain a nontrivial fixed point, which in a lattice formulation such as CDT would appear as a second-order critical point, the approach to which would define a continuum limit. In this work we search the parameter space for such a continuum limit.

An UV limit is obtained by shrinking the lattice spacing a to zero while simultaneously keeping observable quantities fixed in physical units. To give physical meaning to the process of taking an UV limit, we must therefore specify the observable we are fixing in physical units. In this work we use fluctuations of three-volume about de Sitter space and the scaling of the spectral dimension as our physical observables.

Using these two independent methods we find the lattice spacing to be strongly dependent on κ_0, but either independent or only very weakly dependent on Δ. Our results suggest one must maximize κ_0 within phase C in order to take a continuum limit. The C-A transition line defines the set of points for which κ_0 is maximized for each Δ value within

$$\sum_t N_3(t) = N_{(4,1)}.$$

phase C. We therefore propose that one must tune to the C-A transition line in order to take a continuum limit. Using the same logic an IRFP may also then exist when κ_0 is minimized along the transition dividing phase C from the bifurcation phase (see Fig. 7). If this picture is correct a unique RG trajectory would likely follow the path indicated in Fig. 7. This picture is consistent with the finding of Refs. [15,16]; however, further study is needed to confirm or refute this proposal.

APPENDIX A

We derive the proportionality factor in Eq. (8) to be

$$G = \frac{\sqrt{C_4}s_0^2}{3\sqrt{6}} \cdot \Gamma \cdot a_{abs}^2,$$

by analyzing quantum fluctuations of the spatial volume about de Sitter space, as first proposed in Refs. [11,12].

We analyze the relation between (dimensionful) continuous and (dimensionless) discrete spatial volume profiles:

$$\langle V_3(\tau)\rangle = 2\pi^2 \mathcal{R}^3 \cos^3\left(\frac{\sqrt{g_{\tau\tau}}\tau}{\mathcal{R}}\right) = \frac{3}{4}\frac{V_4}{\tilde{s}_0 V_4^{1/4}}\cos^3\left(\frac{\sqrt{g_{\tau\tau}}\tau}{\tilde{s}_0 V_4^{1/4}}\right), \tag{A1}$$

$$\langle N_3(t)\rangle = \frac{3}{4}\frac{N_{(4,1)}}{s_0 N_{(4,1)}^{1/4}}\cos^3\left(\frac{t}{s_0 N_{(4,1)}^{1/4}}\right), \tag{A2}$$

and actions:

$$S_{MS} = \frac{1}{24\pi G}\int d\tau \sqrt{g_{\tau\tau}}\left(\frac{g^{\tau\tau}(\partial_\tau V_3(\tau))^2}{V_3(\tau)}\right.$$
$$\left. + \tilde{\mu}V_3(\tau)^{1/3} - \tilde{\lambda}V_3(\tau)\right), \tag{A3}$$

$$S_{\text{eff}} = \frac{1}{\Gamma}\sum_t\left(\frac{(N_3(t+1) - N_3(t))^2}{N_3(t+1) + N_3(t)} + \mu N_3(t)^{1/3} - \lambda N_3(t)\right), \tag{A4}$$

respectively. In the above expressions $\mathcal{R}$ is the physical radius of the Euclidean de Sitter space (four-sphere) and

$$V_4 = \int d\tau \sqrt{g_{\tau\tau}}V_3(\tau) = \frac{8\pi^2}{3}\mathcal{R}^4 \Rightarrow \tilde{s}_0 = \left(\frac{3}{8\pi^2}\right)^{1/4}.$$

We also have

We assume that the CDT universe (inside phase C) is represented by Euclidean de Sitter space with superimposed quantum fluctuations of the scale factor $a(\tau)$, with a spatially homogeneous and isotropic metric

$$ds^2 = g_{\tau\tau}d\tau^2 + a^2(\tau)d\Omega^3,$$

where $d\Omega^3$ is a line element on an S^3 sphere.

1. Method (a)

Let us assume that consecutive spatial layers of integer time (t and $t+1$) are separated by a universal lattice distance of constant length:

$$a_{\text{time}} = \sqrt{\tilde{\alpha}} \cdot a_{abs} \quad (\tilde{\alpha} = \text{positive const}).$$

By construction, a spatial layer in time t is built of $\frac{1}{2}N_3(t)$ equilateral tetrahedra,[5] each with equal and constant 3-volume $C_3 \cdot a_{abs}^3$, where $C_3 = \frac{\sqrt{2}}{12}$ is the volume of a unit tetrahedron. By construction, the total 4-volume of the CDT universe is

$$V_4 = \sum_t \frac{1}{2}N_3(t)C_3 a_{abs}^3 \, a_{\text{time}} = N_{(4,1)}C_4 a_{abs}^4, \tag{A5}$$

where

$$C_4 \equiv \frac{\sqrt{\tilde{\alpha}}C_3}{2}. \tag{A6}$$

Let us assume that[6]

$$N_3(t) = \frac{\sqrt{g_{\tau\tau}}V_3(\tau)}{C_4 a_{abs}^3}. \tag{A7}$$

By applying ansatz (A7) and relation (A5) to formula (A2) for the discrete volume profile, one indeed obtains

$$\langle V_3(\tau)\rangle = \frac{3}{4}\frac{V_4}{\left(\frac{\sqrt{g_{\tau\tau}}s_0}{C_4^{1/4}}\right)V_4^{1/4}}\cos^3\left(\frac{\sqrt{g_{\tau\tau}}a_{abs}t}{\left(\frac{\sqrt{g_{\tau\tau}}s_0}{C_4^{1/4}}\right)V_4^{1/4}}\right), \tag{A8}$$

which compared to the continuous expression (A1) naturally leads to the identifications

$$\tau \equiv a_{abs}t, \tag{A9}$$

$$\frac{\sqrt{g_{\tau\tau}}s_0}{C_4^{1/4}} \equiv \tilde{s}_0 = \left(\frac{3}{8\pi^2}\right)^{1/4}. \tag{A10}$$

---

[5]See footnote 1.
[6]Note that, as τ is just a (continuous) time coordinate, the physical proper time is given by $\sqrt{g_{\tau\tau}}\tau$, and for the physical 3-volume one should use $\sqrt{g_{\tau\tau}}V_3(\tau)$ rather than $V_3(\tau)$.

Substituting ansatz (A7) into the effective action (A4), one obtains

$$S_{\text{eff}} = \frac{1}{\Gamma} \sum_t \frac{(N_3(t+1) - N_3(t))^2}{N_3(t+1) + N_3(t)} + \cdots$$

$$= \frac{g_{\tau\tau}}{\Gamma C_4 a_{abs}^2} \sum_t \Delta\tau \sqrt{g_{\tau\tau}} \frac{\left(\frac{V_3(\tau+\Delta\tau) - V_3(\tau)}{\sqrt{g_{\tau\tau}}\Delta\tau}\right)^2}{V_3(\tau + \Delta\tau) + V_3(\tau)} + \cdots$$

$$= \frac{g_{\tau\tau}}{2\Gamma C_4 a_{abs}^2} \int d\tau \sqrt{g_{\tau\tau}} \frac{g^{\tau\tau}(\partial_\tau V_3(\tau))^2}{V_3(\tau)} + \cdots, \quad (A11)$$

where we used the identifications $\Delta\tau \equiv a_{abs}$ and $\sum_t \Delta\tau \leftrightarrow \int d\tau$. Comparing Eqs. (A3) and (A11) implies

$$\frac{g_{\tau\tau}}{2\Gamma C_4 a_{abs}^2} = \frac{1}{24\pi G}, \quad (A12)$$

which combined with Eq. (A10) gives the final formula

$$G = \frac{\sqrt{C_4} s_0^2}{3\sqrt{6}} \cdot \Gamma \cdot a_{abs}^2, \quad (A13)$$

where [as defined in Eq. (A6)]

$$C_4 = \frac{\sqrt{2\tilde{\alpha}}}{24} = \text{const.}$$

The absolute lattice spacing calculated using formula (A13) depends on the choice of the dimensionless parameter $\tilde{\alpha}$ which defines the (temporal) lattice spacing between neighboring spatial layers. In this work we are interested in the relative change in lattice spacing when moving between different points in the CDT parameter space, a result that does not depend on the particular choice of $\tilde{\alpha}$. However, in order to compare the absolute lattice spacing with the results obtained by using methods (b) and (c) described below, we choose $\tilde{\alpha} = 5/4$, which sets $C_4 = \sqrt{5}/96$, i.e., equal to the 4-volume of the equilateral unit 4-simplex.

2. Method (b)

We now assume a more realistic picture, where the CDT universe is built of $N_{(4,1)}$ identical (4,1)-simplices and $N_{(3,2)}$ identical (3,2)-simplices, each with physical volume $C_{41} \cdot a_{abs}^4$ and $C_{32} \cdot a_{abs}^4$, respectively. Therefore, Eq. (A5) changes to

$$V_4 = (N_{(4,1)}C_{41} + N_{(3,2)}C_{32})a_{abs}^4 = N_{(4,1)}C_4 a_{abs}^4, \quad (A14)$$

where

$$C_4 \equiv C_{41} + \xi C_{32}, \qquad \xi \equiv \frac{N_{(3,2)}}{N_{(4,1)}}. \quad (A15)$$

The rest of the derivation presented in Method (a) remains intact, so one again arrives at formula (A13). Let us now make a simplifying assumption that all 4-simplices are symmetric and
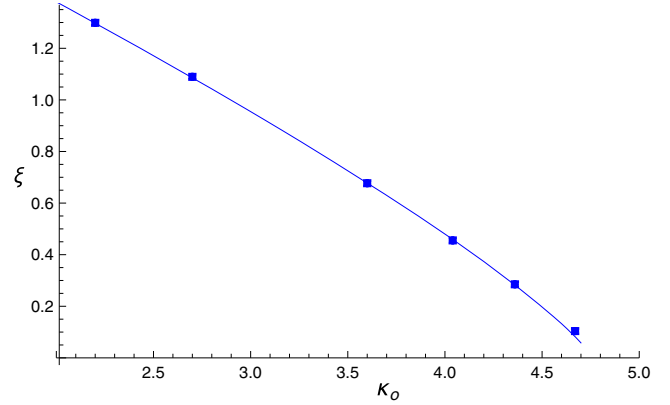

FIG. 8. The dependence of $\xi \equiv \frac{N_{(3,2)}}{N_{(4,1)}}$ on κ_0 for fixed $\Delta = 0.6$. Here, $\xi \to 0$ as one approaches the C-A phase transition observed for $\kappa_0^c \approx 4.7$.

$$C_{41} = C_{32} = \frac{\sqrt{5}}{96},$$

where the numerical value is the volume of a unit equilateral 4-simplex. As a result, we obtain

$$C_4 = \frac{\sqrt{5}}{96}(1 + \xi).$$

Note that for $\xi = 0$ [zero (3,2)-simplices] one recovers the result of Method (a). Actually, as shown in Fig. 8, $\xi \to 0$ as one approaches the C-A phase transition; thus, close to the transition the results of Methods (a) and (b) are very similar.

3. Method (c)

As in Method (b) we assume that the CDT universe is built of both (4,1)- and (3,2)-simplices, but we additionally take into account that $C_{41} \neq C_{32}$. The volume of a 4-simplex is a function of the asymmetry parameter α, defining the ratio of the length of timelike and spacelike links on the lattice ($a_t^2 = \alpha \cdot a_s^2 \equiv \alpha \cdot a_{abs}^2$), and so one has [10][7]

$$C_{41} = \frac{\sqrt{8\alpha - 3}}{96}, \qquad C_{32} = \frac{\sqrt{12\alpha - 7}}{96}. \quad (A16)$$

The asymmetry parameter α is also related to the bare coupling constants κ_0, Δ and κ_4 in the bare Regge-Einstein-Hilbert action of CDT (2),

$$S_E = -(\kappa_0 + 6\Delta)N_0 + \kappa_4(N_{(4,1)} + N_{(3,2)}) + \Delta N_{(4,1)},$$

by the following set of equations [10]:

$$\kappa_0 + 6\Delta = \frac{1}{8G}\sqrt{4\alpha - 1}, \quad (A17)$$

---

[7]Here we use the Wick rotated (Euclidean) version of the formulas in [10], i.e., the one obtained by an analytical continuation of square roots in the lower half of the complex α plane: $\sqrt{-\alpha} = -i\sqrt{\alpha}$.

$$\kappa_4 + \Delta = \frac{\Lambda}{8\pi G}\frac{\sqrt{8\alpha - 3}}{96} + \frac{\sqrt{3}}{8\pi G}\left(\arccos\frac{1}{\sqrt{24\alpha - 8}} - \frac{\pi}{2}\right)$$

$$+ \frac{\sqrt{4\alpha - 1}}{8\pi G}\left(\frac{3}{2}\arccos\frac{2\alpha - 1}{6\alpha - 2} - \frac{\pi}{2}\right), \qquad (A18)$$

$$\kappa_4 = \frac{\Lambda}{8\pi G}\frac{\sqrt{12\alpha - 7}}{96} + \frac{\sqrt{3}}{32\pi G}\arccos\frac{6\alpha - 5}{6\alpha - 2} +$$

$$+ \frac{\sqrt{4\alpha - 1}}{8\pi G}\left(\frac{3}{4}\arccos\frac{4\alpha - 3}{8\alpha - 4}\right.$$

$$+ \frac{3}{2}\arccos\frac{1}{\sqrt{8\alpha - 4}\sqrt{6\alpha - 2}} - \pi\bigg), \qquad (A19)$$

where G and Λ are the bare Newton and cosmological constants, respectively. For given values of κ_0, Δ and κ_4, one can solve Eqs. (A17)–(A19) for α and then use it to calculate C_{41} and C_{32} according to Eq. (A16). Summing up, once again, we obtain formula (A13), but now we have

$$C_4 = \frac{\sqrt{8\alpha - 3}}{96} + \xi\frac{\sqrt{12\alpha - 7}}{96},$$

where $\alpha = \alpha(\kappa_0, \Delta, \kappa_4)$. Unfortunately, it turns out that close to the C-A phase transition (for large κ_0), double-valued or complex α solutions are possible for Eqs. (A17)–(A19). As a result, Method (c) is only valid well inside phase C.

[1] M. H. Goroff and A. Sagnotti, The ultraviolet behavior of Einstein gravity, Nucl. Phys. **B266**, 709 (1986).

[2] S. Weinberg, Ultraviolet Divergences in Quantum Theories of Gravitation, in *General Relativity: An Einstein Centenary Survey*, edited by S. W. Hawking, W. Israel (Cambridge University Press, 1980), pp. 790–831.

[3] M. Reuter and F. Saueressig, Quantum Einstein gravity, New J. Phys. **14**, 055022 (2012).

[4] O. Lauscher and M. Reuter, Ultraviolet Fixed Point and Generalized Flow Equation of Quantum Gravity, Phys. Rev. D **65**, 025013 (2001).

[5] D. F. Litim, Fixed Points of Quantum Gravity, Phys. Rev. Lett. **92**, 201301 (2004).

[6] A. Codello, R. Percacci, and C. Rahmede, Ultraviolet properties of f(R)-gravity, Int. J. Mod. Phys. A **23**, 143 (2008).

[7] A. Codello, R. Percacci, and C. Rahmede, Investigating the ultraviolet properties of gravity with a Wilsonian renormalization group equation, Ann. Phys. (Amsterdam) **324**, 414 (2009).

[8] D. Benedetti, P. F. Machado, and F. Saueressig, Asymptotic safety in higher-derivative gravity, Mod. Phys. Lett. A **24**, 2233 (2009).

[9] T. Regge, General relativity without coordinates, Nuovo Cimento **19**, 558 (1961).

[10] J. Ambjorn, J. Jurkiewicz, and R. Loll, Dynamically triangulating Lorentzian quantum gravity, Nucl. Phys. **B610**, 347 (2001).

[11] J. Ambjorn, A. Gorlich, J. Jurkiewicz, and R. Loll, Planckian Birth of the Quantum de Sitter Universe, Phys. Rev. Lett. **100**, 091304 (2008).

[12] J. Ambjorn, A. Gorlich, J. Jurkiewicz, and R. Loll, The Nonperturbative Quantum de Sitter Universe, Phys. Rev. D **78**, 063544 (2008).

[13] J. Ambjorn, S. Jordan, J. Jurkiewicz, and R. Loll, A Second-Order Phase Transition in CDT, Phys. Rev. Lett. **107**, 211303 (2011).

[14] J. Ambjorn, J. Gizbert-Studnicki, A. Gorlich, and J. Jurkiewicz, The effective action in 4-dim CDT. The transfer matrix approach, J. High Energy Phys. 06 (2014) 034.

[15] J. Ambjorn, A. Gorlich, J. Jurkiewicz, A. Kreienbuehl, and R. Loll, Renormalization group flow in CDT, Classical Quantum Gravity **31**, 165003 (2014).

[16] D. N. Coumbe and J. Jurkiewicz, Evidence for asymptotic safety from dimensional reduction in causal dynamical triangulations, J. High Energy Phys. 03 (2015) 151.

[17] J. Ambjørn, A. Görlich, J. Jurkiewicz, R. Loll, J. Gizbert-Studnicki, and T. Trześniewski, The semiclassical limit of causal dynamical triangulations, Nucl. Phys. **B849**, 144 (2011).

[18] J. Ambjorn, J. Jurkiewicz, and R. Loll, Spectral Dimension of the Universe, Phys. Rev. Lett. **95**, 171301 (2005).

[19] G. Giasemidis, J. F. Wheater, and S. Zohren, Dynamical Dimensional Reduction in Toy Models of 4D Causal Quantum Gravity, Phys. Rev. D **86**, 081503 (2012).

[20] J. Ambjorn, S. Jordan, J. Jurkiewicz, and R. Loll, Second- and First-Order Phase Transitions in CDT, Phys. Rev. D **85**, 124044 (2012).